Catalysis Science & Technology

Accepted Manuscript

This is an *Accepted Manuscript*, which has been through the Royal Society of Chemistry peer review process and has been accepted for publication.

Accepted Manuscripts are published online shortly after acceptance, before technical editing, formatting and proof reading. Using this free service, authors can make their results available to the community, in citable form, before we publish the edited article. We will replace this *Accepted Manuscript* with the edited and formatted *Advance Article* as soon as it is available.

You can find more information about *Accepted Manuscripts* in the Information for Authors.

Please note that technical editing may introduce minor changes to the text and/or graphics, which may alter content. The journal's standard Terms & Conditions and the Ethical guidelines still apply. In no event shall the Royal Society of Chemistry be held responsible for any errors or omissions in this *Accepted Manuscript* or any consequences arising from the use of any information it contains.

ROYAL SOCIETY OF CHEMISTRY

www.rsc.org/catalysis

Hydrodeoxygenation of Propanoic Acid over Silica-Supported Palladium: Effect of Metal Particle Size

Yuliana K. Lugo-José, John R. Monnier, Andreas Heyden
and Christopher T. Williams*

Department of Chemical Engineering, University of South Carolina, Columbia, SC 29208

* To whom correspondence should be addressed:

Christopher T. Williams
Department of Chemical Engineering
Swearingen Engineering Center
University of South Carolina
Columbia, SC 29208
Phone: (803)777-0143
Fax: (803)777-8265
E-mail: willia84@cec.sc.edu

Catalysis Science and Technology
Submitted May 9, 2014

Catalysis Science & Technology Accepted Manuscript

Abstract

The effects of metal nanoparticle size on the hydrodeoxygenation (HDO) of propanoic acid (PAc) over Pd/SiO_2 catalysts was investigated. Strong electrostatic adsorption (SEA) was used to prepare catalysts with Pd nanoparticles ranging between 1.9 to 12.4 nm. The particle sizes were determined by chemisorption (O_2-H_2 titration) and transmission electron microscopy (STEM). The HDO was carried out in a continuous gas-phase reactor at 200ºC and 1 atm at differential conversion. The reaction followed decarbonylation and hydrogenation pathways to yield ethane (C_2H_6) and propionaldehyde (EtCHO), respectively. While the catalytic TOF remained constant between 3.0-12.4 nm it decreased by a factor of 2-3 with decreasing particle size down to 1.9 nm. The reaction rate is therefore considered to be largely structure-insensitive over the range studied. The selectivity toward EtCHO increased as the particle size increased, indicating hydrogenation is favored on single crystal Pd(111) and Pd(100) planes versus corners and edges. For decarbonylation to produce C_2H_6, reaction rate orders with respect to PAc (~0.5) and H_2 (~0), and the apparent activation energy (~12 Kcal/mole), were found to be the same for both 2.0 and 12.4 nm particle sizes. In contrast, the reaction rate order with respect to PAc (~1.0) and H_2 (~0.3) was different for hydrogenation to produce EtCHO. These differences are explained by a change in the rate-determining step for the HDO of propanoic acid.

Catalysis Science & Technology Accepted Manuscript

1. Introduction

The upgrading of biomass-derived pyrolysis oil can provide a means to produce both useful fuels and chemicals, as well as generate substantial economic and environmental benefits. [1, 2] However, such bio-oils contains large amounts of carboxylic acids (e.g., acetic acid, propanoic acid) that decrease stability, are highly corrosive, and are challenging to deoxygenate. [3] Furthermore, fatty acids, fatty acid esters, and triglycerides are present in other sources such as waste greases and nonfood oils from a variety of plants. Therefore, the hydrodeoxygenation (HDO) of biomass-derived carboxylic acids is of both fundamental and practical interest. A significant amount of effort in these areas has focused on catalytic HDO of aliphatic acids using a variety of monometallic and bimetallic catalysts. [3-25]

Previous studies have shown that the physical properties of small catalytic nanoparticles are often significantly different from those of bulk metals.[26-31] Research over the years has suggested that particle size-induced changes in the electronic structure and/or the geometry of the metal atoms exposed at the catalyst surface will influence catalyst performance. [32] Along these lines, Boudart et al. classified catalytic reactions as either structure-sensitive or structure-insensitive. [33] If the reaction is structure-insensitive and there are no mass transport limitations, the active sites will be proportional to the number of surface metal atoms, regardless of metal nanoparticle size. However, if the reaction is structure-sensitive the turnover frequency (TOF) changes as the metal dispersion is altered. For example, reactions such as the hydrodechlorination of 1,2-dichloroethane over Pd/SiO_2, are considered to be structure-insensitive. [34] In contrast, reactions over Pd/SiO_2 such as hydrogenolysis of methylcyclopropane, hydrogenation of ethylene, and

Catalysis Science & Technology Accepted Manuscript

selective hydrogenation of acetylene in ethylene-rich mixtures are considered structure-sensitive.[35-38]

Interestingly, there has been very little work performed to explore the structure sensitivity of aliphatic acid HDO over metals. In the only such study, Simakova et al. [14] investigated the effect of metal dispersion on the deoxygenation of palmitic and stearic acid over Pd/C catalysts in the liquid phase. The initial TOF varied by almost an order of magnitude when the initial dispersion of a 1%Pd catalyst was varied from 18% to 72%. However, only four particle sizes were examined, and the catalysts (especially the one with highest dispersion) were found to greatly sinter during the reaction.

The present work explores the effects of metal nanoparticle size (1.9-12.4 nm) on the HDO of propanoic acid (PAc) over a family of silica-supported palladium catalysts. While some small effects on catalytic performance are observed, the activity and selectivity of HDO is not influenced significantly by Pd particle size in the range studied, suggesting that the reaction is largely structure insensitive.

2. Experimental Methods

2.1 Catalyst Synthesis

The Pd/SiO_2 catalysts were synthesized by strong electrostatic adsorption (SEA), where the pH of the metal salt complex solution (100-400 ppm of $[Pd(NH_3)_4]^{2+}Cl_2$, 99.9% Sigma Aldrich) was controlled based on the potential of zero charge (PZC) of the SiO_2. [39, 40] Once the pH of 11.5 was acquired, the support (Aerosil 300 or 130, Evonik, see details below) was impregnated and shaken for 1 hour at room temperature. The surface loading of the catalyst support ranged from 1000-2000 m^2/L. Additional details about the SEA procedure are

Catalysis Science & Technology Accepted Manuscript

explained elsewhere.[41-44] For some Pd catalysts, thermal pre-treatments were performed on Aerosil 300 SiO_2 support prior to SEA in order to assist in achieving different Pd particle sizes (see Table 1). For Pd-6, Aerosil 130 SiO_2 was used. The catalysts were dried overnight, and pre-treated at different conditions in 20% H_2/balance He in order to obtain a range of different particle sizes through sintering. The final treatment stage prior to reaction involved *in-situ* reduction in 20% H_2/balance He for 2 hours at 350ºC. Table 2 summarizes the prepared Pd/SiO_2, which were named Pd-1 to Pd-10 based on their increasing particle size.

2.2 Catalyst Characterization

2.2.1 Pulsed H_2 Titration of Oxygen Pre-Covered Sites

The dispersions and particle sizes of the catalysts were determined by pulsed hydrogen titration of oxygen pre-covered sites utilizing a Micromeritics 2920 AutoChem II Analyzer. The catalysts (0.1-0.2g) were reduced at 350 ºC by flowing 20% H_2/balance He, for 2 hrs, followed by purging with Ar for 1 hr to remove the physisorbed hydrogen. After cooling to 40 ºC in flowing Ar, the catalysts were exposed to 10% O_2/He for 30 min followed by purging with Ar (30 min). Titration with pulses of 10% H_2/Ar was then employed until no further H_2 uptake occurred.

2.2.2 Transmission Electron Microscopy

Scanning transmission electron microscopy (STEM) was performed on a JEOL 2100F 200kV FEG-STEM/TEM equipped with a CEOS C_s corrector on the illumination system. The geometrical aberrations were measured and controlled to provide less than a $\pi/4$ phase shift of the incoming electron wave over the probe-defining aperture of 17.5 mrad, which at 200kV provides a nominal probe size of <0.1nm. High angle annular dark-field (HAADF) STEM images were acquired on a Fischione Model 3000 HAADF detector with a camera length such

Catalysis Science & Technology Accepted Manuscript

that the detector spanned 50-284 mrad. The scanning acquisition was synchronized to the 60 Hz AC electrical power to minimize 60Hz noise in the images and a pixel dwell time of 15.8µs was chosen. Histograms of the particle size distribution were obtained by measuring particles from at least six different micrographs for any sample analyzed.

2.3 Catalyst Evaluation

All activity and kinetics measurements for the HDO of PAc were carried out under atmospheric pressure in a single pass, packed bed, plug flow reactor system with online GC analysis. Prior to the reaction, the catalysts (~0.2 g) were reduced *in-situ* (as indicated in Table 1) at a total flow of 200 sccm for 2 hours in 20% H_2 balance He. All the catalytic activity experiments were conducted at 200ºC, with 1.0% PAc (Alfa Aesar, 99%) and 20% H_2, balance He. The reaction rate was determined based on the formation of product (which is proportional to the rate of acid disappearance) in µmol product formed/min•gcat and turnover frequencies were based on the reaction rate per active site based on surface atoms (TOF, molecules•site^{-1}min^{-1}). For the kinetic experiments, PAc and H_2 mole fractions ranged from X_{PAc} ~ 0.0020-0.017 and X_{H2} ~ 0.20-0.99. Measurements were also carried out from 200-240 ºC in order to determine the apparent activation energy. The plug flow reactor system, including gas chromatographic analysis of product streams, is the same as described previously.[41] The conversion and selectivity for a given catalyst were defined according to the following equations:

$$Conversion = \left(\frac{\sum P_i / \lambda_i}{PAc_{in}} \right) * 100$$

$$Selectivity\ of\ Product\ i = \frac{TOF_{Pi}}{\sum_{i}^{n} TOF_{Pi}}$$

Catalysis Science & Technology Accepted Manuscript

where PAc_{in} denotes the concentration of PAc in the feed, TOF_{Pi} is the turnover frequency for a given product, and λ_i and P_i are the stoichiometric factors and product concentrations, respectively. Experiments were carried out at differential conversion in the kinetic regime, under conditions confirmed to be free of both internal (Fig. S1) and external (Fig. S2) mass transfer limitations (see Supporting Information).

3. Results and Discussion

3.1 Particle Size Characterization

In order to be able to draw clear correlations between structure and catalytic performance, the intrinsic catalyst properties such as dispersion, surface active sites, and particle size had to be determined. As summarized in Table 2, two characterization techniques were employed: chemisorption (O_2-H_2 titration), and STEM, with the latter applied to both the fresh and spent catalyst (i.e., before and after the reaction). A wide range of particle sizes and dispersions ranging from 1.9-12.4 nm was obtained by O_2-H_2 titration. Representative STEM images are shown in Figure 1 for the Pd-2, Pd-6 and Pd-10 catalysts, both before and after reaction, with Figure 2 showing the associated histograms**.** The Sauter mean particle size was determined from the surface area based on the measured Pd crystallite size distribution. The estimated particle size for the fresh and spent Pd-2 catalyst was 2.7±0.9 and 2.8±0.7 nm, respectively, which is in excellent agreement with chemisorption. For Pd-6, particle sizes of 5.1±1.1 and 8.0±2.0 nm were found for the fresh and spent catalyst, respectively. Finally, the size of the fresh Pd-10 (12.1±2.7 nm) was not significantly effected after the reaction (13.4±3.5 nm) and was in close agreement with chemisorption (d_{Pd} =12.4 nm). Additionally, the DeBrouckere mean particle size calculated from STEM was compared with that estimated by XRD, showing good agreement (see

Catalysis Science & Technology Accepted Manuscript

Supporting Information S1.2). Given the inherent assumptions and limitations (e.g., ideal particle shape, [45] relatively small sampling of particles in microscopy) in the calculations associated with these techniques, the agreement is relatively good overall. Since chemisorption can count all exposed surface Pd sites in each sample, the estimate of particle size and dispersion from this approach was used to obtain the TOF values for this study.

3.2 Particle Size Effect on Activity and Selectivity

In order to elucidate the effect of metal particle size for the HDO of PAc, the activity and selectivity of each Pd/SiO_2 catalyst was investigated under the same conditions. The specific activity expressed per Pd surface atom (TOF) and selectivity towards C_2H_6 and propionaldehyde (EtCHO) are summarized in Table 3. Starting at the smallest particle size, the overall TOF increased by around a factor of 2.5 up to 3.1 nm, above which point it remained roughly constant. The overall change over the whole range is considerably less than the differences in other well-known structure sensitive reactions. [35, 46, 47] This point will be addressed in the next section. From 1.9 to 3.1 nm, the selectivity is found to be >90% toward C_2H_6, with the balance going towards EtCHO. Thus, in this size range, the HDO of PAc occurs primarily via decarbonylation and subsequent hydrogenation (pathway 2 in Scheme 1) to form the main products C_2H_6 and CO. Further increase in the particle size up to 12.4 nm shifted the selectivity toward EtCHO up to about 24% (balance C_2H_6).

These trends can be further analyzed by examining the change in the TOF for production of each product with particle size, as shown in Table 3. The general trend is that the C_2H_6 TOF increases more at the lowest particle size range, while the EtCHO increases more at the higher particle size range. To attempt to quantify the trends in product formation and further explore structure

Catalysis Science & Technology Accepted Manuscript

sensitivity, the following analysis was performed. Given the f.c.c. crystal structure of Pd and assuming the particles are shaped as cubo-octahedra with corners truncated as (100) planes, Van Hardeveld and Hartog [48] statistics can be applied. This assumption is reasonable, given that XRD of the catalysts (Fig. S4, Supplemental Information) and high resolution STEM of the small particles in the Pd-2 and Pd-6 samples (Fig. S5, Supplemental Information) show that the Pd is crystalline in nature. As a result, the amount of (111) and (100) planes can be estimated based on the Pd particle sizes. Table 3 summarizes the fraction (in percent) of (111) and (100) planes found in these samples. In the range from 1.9 to 3.1 nm where the largest change in overall TOF occurs, the combined fraction of (111) and (100) planes changes from 56% to 71%, with low coordination sites such as corners and edges making up the significant fraction of the remaining surface. As the particle size increases beyond 3.1 up to 12.4 nm, the combined fraction of (111) and (100) planes increases from 71 to 93%, at which point the low coordinated sites are greatly diminished.

For the purposes of this analysis, it was hypothesized that the TOF value for each product will be different on each of these types of surface sites (i.e., (111), (100), corners/edges). If this is the case, then the TOF values for each product can be written as:

$$TOF_{C2H6} = TOF_{C2H6/(111)} \times F_{(111)} + TOF_{C2H6/(100)} \times F_{(100)} + TOF_{C2H6/CE} \times F_{CE}$$

$$TOF_{EtCHO} = TOF_{EtCHO/(111)} \times F_{(111)} + TOF_{EtCHO/(100)} \times F_{(100)} + TOF_{EtCHO/CE} \times F_{CE}$$

where, TOF_{C2H6} and TOF_{EtCHO} are the total TOF values for those products, $TOF_{i/j}$ are the TOF values for the given molecule i = C_2H_6, EtCHO, on a given type of site j = Pd(111), Pd(100), Pd corners/edges (CE), and F_j are the fractions of each type of site. Using the experimental data for the ten catalysts in Table 3 and assuming that TOF values on various types of sites are

Catalysis Science & Technology Accepted Manuscript

independent of particle size, the values of $TOF_{i/j}$ were estimated by using least squares regression.

Figure 3 shows the estimated total TOF values for each product (lines) compared with the experimental data (points), along with the fitted values of $TOF_{i/j}$. It is seen that the decarbonylation of PAc to produce C_2H_6 is favorable on both Pd(111) and Pd(100) faces but not on corners/edges. In addition, the production of EtCHO would appear to be favored on Pd(100) sites. While admittedly somewhat speculative, this analysis helps to rationalize the very small particle size effect over the range studied. The reaction takes place mainly on Pd(111) and Pd(100) sites, which increase by 75% over the range studied. In contrast, the almost 7-fold decrease in the fraction of corners/edges sites has a negligible effect on activity due to their inactivity for this reaction.

The analysis above uses the initial dispersion obtained by chemisorption to calculate TOF values and associated estimated particle sizes. However, as indicated by the STEM for Pd-6 (Figs. 1 and 2), some of the samples are likely to have experienced some sintering during the reaction. In this event, some data points in Figure 3 would be shifted to higher particle size, and larger TOF values. However, the estimated TOF values for surface sites arising from (111), (100), and kinks/edges would not be changed significantly, and general trends described above would still hold. In particular, the inactivity of the kink/edge sites is clear regardless of the assumptions made in the analysis.

As mentioned earlier, a previous particle size effect study involving deoxygenation of palmitic and stearic acid over 1 wt% Pd/C was conducted by Simakova et al.[14] Their results suggested that as the Pd dispersion increased up to 65%, there was an increase in the TOF. However, for

Catalysis Science & Technology Accepted Manuscript

72% disperse catalyst, there was a significant (~10-fold) decrease in the TOF, attributed to the extreme sintering that occurred in that sample based on post reaction characterization. The present results would seem to contradict these previous findings, since overall activity decreased with increasing dispersion and there was no significant sintering at the lowest dispersion. Further studies are required to determine if the origin of these differences is from the support (SiO_2 vs. C) or reaction environment (gas-phase vs. liquid-phase).

3.3 Particle Size Effect on Kinetics

The reaction kinetics for the Pd-10 (12.4nm) catalyst were explored using a power rate law equation, $TOF_i = A_i \exp\left(-\frac{Ea_i}{RT}\right)\left(\prod_{i=1}^{n} X_i^{\alpha_i}\right)P^{\Sigma_{i=1}^{n}\alpha_i}$, where A_i is the pre-exponential factor, Ea_i is the apparent activation energy, X_i are the mole fractions of species i, P is the total pressure in the reactor, α_i is the reaction order of species i, and TOF_i is the rate of production of species i in terms of turnover frequency. The reaction orders can be obtained from the slope of ln TOF vs. ln X_i of PAc and H_2 (i.e., X_{PAc} and X_{H2}, respectively). Figure 4 shows that the reaction orders for the TOF_{C2H6} on Pd-10 with respect to PAc and H_2 are approximately 0.5 and 0, respectively, over the concentration range examined. These reaction orders are consistent with our previous study [41] of the Pd-2 (2 nm) catalyst, which produces essentially only C_2H_6 as a product (cf. Table 3). In addition, the results are in harmony with the computational studies of Heyden [49] for the decarbonylation (DCN) of PAc on Pd(111) model surfaces. Their findings indicated that a α-carbon dehydrogenation followed by dehydroxylation to produce CH_3CHCO is required to promote C-CO bond scission to yield CO and C2 hydrocarbons. The extent and removal of the hydrocarbon pool (CH_3CH_x) at the surface, explains why the reaction order with respect to PAc

Catalysis Science & Technology Accepted Manuscript

is less than one. Based on these results, it is concluded that the rate-determining step for the DCN reaction is essentially the same for all the particle sizes studied.

In contrast, the TOF_{EtCHO} exhibits reaction rate orders for PAc and H_2 of approximately 1.0 and 0.3, respectively, over the range of concentrations examined. The reason for the different reaction rate orders (with respect to PAc and H_2) for the two products formed can be explained by the two reaction pathways PAc undergoes. For the formation of C2's hydrocarbons, the preferred reaction pathway is DCN (CO and C2's), whereas for the formation of EtCHO the preferred reaction pathway is hydrogenation (without carbon loss). In the latter pathway, a Langmuir Hinshelwood-type adsorption sequence is assumed with PAc and H_2 adsorbing dissociatively mainly on Pd(100) sites and combining to form propionyl and/or acetal intermediates. The subsequent hydrogenation of propionyl and/or acetal species leads to the formation of EtCHO. Therefore, the hydrogenation to produce EtCHO would be expected to have a 1^{st} order dependence with respect to PAc.

With respect to the concentration of H_2, a reaction order of 0.3 depends on what reaction pathway is favorable. The addition of hydrogen to form an acetal intermediate results in a reaction rate order of ~0.5, due to the assumption of equilibrated hydrogen adsorption on the surface. Alternatively, the –OH bond scission to form propionyl would result in an H_2 reaction rate order of ~0 will be expected. Both of these intermediates further react to form the EtCHO product. Thus, if both pathways occur to some extent, the rate order with respect to hydrogen would be expected to be between 0-0.5, consistent with the experimental observation. We are currently exploring the reaction pathways over Pd(110) using computational studies to further

Catalysis Science & Technology Accepted Manuscript

probe the mechanism. It should be noted that the propionyl species can also undergo decarbonlyation to produce the C2 species that are responsible for the formation of ethane.

The Arrhenius plot for the TOF of Pd-10 (12.4nm) is shown in Figure 5. An apparent activation energy value of 11.7 ± 0.3 is found for C_2H_6/EtCHO production, which is same as observed in our previous detailed study of Pd-2 (2 nm). [41] This again suggests a similar rate determining step for C_2H_6 and EtCHO production occurring on the Pd(111) and Pd(100) sites present in these catalysts.

4. Conclusion

The present findings shed new light on the influence of metal particle size on the HDO of aliphatic carboxylic acids. Activity and selectivity trends for a family of Pd/SiO_2 catalysts at 200ºC revealed that PAc decarbonylation was the favored pathway over the entire particle size range studied (1.9-12.4 nm). While the reaction appears to be not strongly structure sensitive, some instructive trends in catalytic performance were observed. Smaller particles are less active but highly selective toward the formation of C_2H_6, whereas larger particles are more active but shift the selectivity partly toward EtCHO. These differences are attributed primarily to the differing composition of Pd crystal facets exposed in these catalysts, and suggest a means of tuning the selectivity through controlling particle size and shape. Current HDO studies in our laboratory are focusing on exploring such particle size effects for other transition metals, as well as the use of bimetallic catalysts to enhance activity and stability.

5. Acknowledgments

The authors wish to thank the financial support from National Science Foundation (NSF) grant number CHE-1153012. Yuliana Lugo-José thanks the Sloan Foundation and the NSF

Catalysis Science & Technology Accepted Manuscript

Southeastern Alliance for Graduate Education and the Professoriate (SEAGEP) for financial support. At the University of South Carolina, the authors thank Professor John R. Regalbuto for his helpful and insightful conversations regarding catalyst synthesis; Dr. Douglas Blom for TEM analysis; Prof. Hanno Zur Loye for the use of his XRD equipment; and Sina Behtash for interesting discussions related to mechanistic aspects of this reaction system.

Catalysis Science & Technology Accepted Manuscript

6. References

1. D. Kubicka, I. Kubicková and J. Čejka, *Catalysis Reviews*, 2013, **55**, 1-78.
2. A. V. Bridgwater, D. Meier and D. Radlein, *Organic Geochemistry*, 1999, **30**, 1479-1493.
3. T. N. Pham, D. Shi and D. E. Resasco, *Applied Catalysis B: Environmental*, 2014, **145**, 10-23.
4. J. C. Serrano-Ruiz, A. Pineda, A. M. Balu, R. Luque, J. M. Campelo, A. A. Romero and J. M. Ramos-Fernández, *Catalysis Today*, 2012, **195**, 162-168.
5. B. J. O'Neill, E. I. Gürbüz and J. A. Dumesic, *Journal of Catalysis*, 2012, **290**, 193-201.
6. C. A. Henao, D. Braden, C. T. Maravelias and J. A. Dumesic, in *Computer Aided Chemical Engineering*, eds. M. C. G. E.N. Pistikopoulos and A. C. Kokossis, Elsevier, 2011, vol. Volume 29, pp. 1723-1727.
7. R. M. West, E. L. Kunkes, D. A. Simonetti and J. A. Dumesic, *Catalysis Today*, 2009, **147**, 115-125.
8. J. Q. Bond, D. Wang, D. M. Alonso and J. A. Dumesic, *Journal of Catalysis*, 2011, **281**, 290-299.
9. S. G. Wettstein, J. Q. Bond, D. M. Alonso, H. N. Pham, A. K. Datye and J. A. Dumesic, *Applied Catalysis B: Environmental*, 2012, **117–118**, 321-329.
10. E. W. Ping, J. Pierson, R. Wallace, J. T. Miller, T. F. Fuller and C. W. Jones, *Applied Catalysis A: General*, 2011, **396**, 85-90.
11. S. J. Tauster, S. C. Fung and R. L. Garten, *J Am Chem Soc*, 1978, **100**, 170-175.
12. T. C. Chang, J. J. Chen and C. T. Yeh, *Journal of Catalysis*, 1985, **96**, 51-57.
13. S. J. Tauster, *Accounts of Chemical Research*, 1987, **20**, 389-394.
14. I. Simakova, O. Simakova, P. Mäki-Arvela, A. Simakov, M. Estrada and D. Y. Murzin, *Applied Catalysis A: General*, 2009, **355**, 100-108.
15. H. Bernas, K. Eränen, I. Simakova, A.-R. Leino, K. Kordás, J. Myllyoja, P. Mäki-Arvela, T. Salmi and D. Y. Murzin, *Fuel*, 2010, **89**, 2033-2039.
16. D. Y. Murzin, M. Snare, I. Kubickova, P. Maki-Arvela, K. Eranen and J. Warna, *Chem Eng J*, 2007, **134**, 29-34.
17. S. Lestari, I. Simakova, A. Tokarev, P. Mäki-Arvela, K. Eränen and D. Murzin, *Catalysis Letters*, 2008, **122**, 247-251.
18. S. Lestari, P. Mäki-Arvela, I. Simakova, J. Beltramini, G. Lu and D. Murzin, *Catalysis Letters*, 2009, **130**, 48-51.
19. I. Kubicková, M. Snåre, K. Eränen, P. Mäki-Arvela and D. Y. Murzin, *Catalysis Today*, 2005, **106**, 197-200.
20. J. N. Chheda and J. A. Dumesic, *Catalysis Today*, 2007, **123**, 59-70.
21. M. Chia and J. A. Dumesic, *Chemical Communications*, 2011, **47**, 12233-12235.
22. K. Jacobson, K. C. Maheria and A. Kumar Dalai, *Renewable and Sustainable Energy Reviews*, 2013, **23**, 91-106.
23. M. Mohammad, T. Kandaramath Hari, Z. Yaakob, Y. Chandra Sharma and K. Sopian, *Renewable and Sustainable Energy Reviews*, 2013, **22**, 121-132.
24. E. Furimsky, *Catalysis Today*, 2013, **217**, 13-56.
25. M. Snåre, I. Kubičková, P. Mäki-Arvela, K. Eränen and D. Y. Murzin, *Industrial & Engineering Chemistry Research*, 2006, **45**, 5708-5715.
26. G. C. Bond, *Surface Science*, 1985, **156, Part 2**, 966-981.

Catalysis Science & Technology Accepted Manuscript

27. C. R. Henry, C. Chapon, S. Giorgio and C. Goyhenex, in *Chemisorption and Reactivity on Supported Clusters and Thin Films*, eds. R. Lambert and G. Pacchioni, Springer Netherlands, 1997, vol. 331, pp. 117-152.
28. P. E. Strizhak, *Theor Exp Chem*, 2013, **49**, 2-21.
29. C. P. Vinod, *Catalysis Today*, 2010, **154**, 113-117.
30. B. R. Cuenya, *Thin Solid Films*, 2010, **518**, 3127-3150.
31. F. Zaera, *Prog Surf Sci*, 2001, **69**, 1-98.
32. J. M. Martínez de la Hoz and P. B. Balbuena, *The Journal of Physical Chemistry C*, 2011, **115**, 21324-21333.
33. M. Boudart, *Chemical Reviews*, 1995, **95**, 661-666.
34. S. Lambert, C. Cellier, P. Grange, J.-P. Pirard and B. t. Heinrichs, *Journal of Catalysis*, 2004, **221**, 335-346.
35. J. B. Butt and C. L. M. Joyal, *Journal of the Chemical Society, Faraday Transactions*, 1990, **86**, 2911-2917.
36. N. Marín-Astorga, G. Pecchi, J. L. G. Fierro and P. Reyes, *Catalysis Letters*, 2003, **91**, 115-121.
37. A. Borodziński, *Catalysis Letters*, 2001, **71**, 169-175.
38. A. Binder, M. Seipenbusch, M. Muhler and G. Kasper, *Journal of Catalysis*, 2009, **268**, 150-155.
39. T. E. Feltes, L. Espinosa-Alonso, E. d. Smit, L. D'Souza, R. J. Meyer, B. M. Weckhuysen and J. R. Regalbuto, *Journal of Catalysis*, 2010, **270**, 95-102.
40. R. John, in *Catalyst Preparation*, CRC Press, 2006, pp. 297-318.
41. Y. K. Lugo-José, J. R. Monnier and C. T. Williams, *Applied Catalysis A: General*, 2014, **469**, 410-418.
42. S. Lambert, N. Job, L. D'Souza, M. F. R. Pereira, R. Pirard, B. Heinrichs, J. L. Figueiredo, J.-P. Pirard and J. R. Regalbuto, *Journal of Catalysis*, 2009, **261**, 23-33.
43. L. Jiao and J. R. Regalbuto, *Journal of Catalysis*, 2008, **260**, 329-341.
44. J. T. Miller, M. Schreier, A. J. Kropf and J. R. Regalbuto, *Journal of Catalysis*, 2004, **225**, 203-212.
45. O.-L. Pérez, D. Romeu and M. J. Yacamán, *Journal of Catalysis*, 1983, **79**, 240-241.
46. N. D. Spencer, R. C. Schoonmaker and G. A. Somorjai, *Nature*, 1981, **294**, 643-644.
47. A. V. Zeigarnik, R. E. Valdés-Pérez and O. N. Myatkovskaya, *The Journal of Physical Chemistry B*, 2000, **104**, 10578-10587.
48. R. Van Hardeveld and F. Hartog, *Surface Science*, 1969, **15**, 189-230.
49. J. Lu, S. Behtash, M. Faheem and A. Heyden, *Journal of Catalysis*, 2013, **305**, 56-66.

Catalysis Science & Technology Accepted Manuscript

Figures and Tables

Table 1. SiO_2 thermal treatment conditions and resulting surface areas for synthesized catalysts.

Support SA (m^2/g)	**Support Heat Treatment Cond.**	**Catalyst Id.**	**Pd loading (wt%)**
330	Not heat treated	Pd-1	2.0
330		Pd-2	4.0
330		Pd-3	2.6
309	350ºC, 2hrs, helium	Pd-4	2.0
190	800ºC, 24hrs, calcined	Pd-5	1.4
130		Pd-6	1.9
285	500ºC, 2hrs, hydrogen	Pd-7	3.5
285		Pd-8	3.5
190	800ºC, 24hrs, calcined	Pd-9	2.9
309	350ºC, 2hrs, helium	Pd-10	3.3

Catalysis Science & Technology Accepted Manuscript

Table 2. Physical properties of Pd/SiO_2 catalysts.

Catalyst Id.	Pd loading (wt%)	Pre-treatment cond.[b] 20% H_2/bal. He	Disp.[a] (%)	d_{Pd}[a] (nm) O_2-H_2 titr.	d_{Pd} (nm) TEM (after)[c]
Pd-1	2.0	150ºC, 2.5ºC/min, 2hrs	58.6	1.9	2.7(2.8)
Pd-2	4.0		55.7	2.0	
Pd-3	2.6		53.7	2.1	
Pd-4	2.0		43.1	2.6	
Pd-5	1.4		36.4	3.1	
Pd-6	1.9		29.4	3.8	5.1(8.0)
Pd-7	3.5		18.1	6.2	
Pd-8	3.5	400ºC, 10ºC/min, 2hrs	14.3	7.9	
Pd-9	2.9	150ºC, 2.5ºC/min, 2hrs	11.6	9.7	
Pd-10	3.3	350ºC, 2.5ºC/min, 2hrs	9.0	12.4	12.1(13.4)

[a] Determined by chemisorption, O_2-H_2 titration. [b] Catalysts were reduced *in-situ* at 350ºC, for 2 hours at 5ºC/min, unless otherwise noted. [c] TEM results in parenthesis indicate the particle size obtained after the reaction.

Catalysis Science & Technology Accepted Manuscript

Table 3. Kinetic data[a] for HDO of PAc over Pd/SiO_2 catalysts.

Cat. Id.	d_{pd} (nm) O_2-H_2 titr.	Overall TOF (min^{-1})	EtCHO Select.	C_2H_6 Select.	EtCHO TOF (min^{-1})	C_2H_6 TOF (min^{-1})	Face (111)[b] (%)	Face (100)[b] (%)
Pd-1	1.9	0.51	0.08	0.92	0.05	0.46	47	6
Pd-2	2.0	0.38	0.05	0.95	0.05	0.34	49	6
Pd-3	2.1	0.56	0.09	0.91	0.05	0.51	50	7
Pd-4	2.6	0.67	0.06	0.94	0.10	0.57	56	9
Pd-5	3.1	0.89	0.04	0.96	0.04	0.85	60	11
Pd-6	3.8	0.92	0.16	0.85	0.11	0.81	64	12
Pd-7	6.2	0.95	0.09	0.91	0.08	0.87	70	15
Pd-8	7.9	0.84	0.17	0.83	0.13	0.71	72	16
Pd-9	9.7	0.87	0.16	0.84	0.13	0.74	74	17
Pd-10	12.4	0.95	0.24	0.76	0.22	0.73	75	18

[a] Conditions: T = 200 ºC; P = 1 atm; ~1.0 % PAc, 20% H_2 balanced with He; catalyst mass = 200 mg; total flow rate = 200 sccm. [b] Van Hardeveld and Hartog[47] statistics on Pd(111) and Pd(100) fraction for the Pd, f.c.c Cubo-Octahedron-corners truncated at (100).

Catalysis Science & Technology Accepted Manuscript

Scheme and Figure Captions

Scheme 1. Reaction pathway for the decarbonylation(DCN)/hydrogenation of PAc over Pd/SiO_2

Figure 1. TEM images for Pd-2 before (A) and after (B) reaction, Pd-6 before (C) and after (D) reaction, and Pd-10 before (E) and after (F) reaction.

Figure 2. Histograms showing the particle size distributions of Pd-2 before (A) and after (B) reaction, Pd-6 before (C) and after (D) reaction, and Pd-10 before (E) and after (F) reaction. N = Number of particles meaured; D_{VSMD} = volume-surface mean diameter; Stdev = standard deviation.

Figure 3. TOF_{C2H6} (squares) and TOF_{EtCHO} (diamonds) as a function of particle size for the series of Pd/SiO_2 catalysts for the HDO of PAc. Reactor conditions: T = 200 ºC; P = 1 atm; ~1.0 % PAc, 20% H_2 balanced with He; catalyst mass = 200 mg; total flow rate = 200 sccm. The solid lines are the least squares fits of the data. See text for details.

Figure 4. Power rate law dependencies of TOF_{C2H6} (squares) and TOF_{EtCHO} (diamonds) on PAc (filled symbols) and H_2 (open symbols) over Pd-2 (red symbols, bottom plot) and Pd-10 (black symbols, top plot). Reactor conditions: T = 200 ºC; P = 1 atm; PAc, 20% H_2 balanced with He; catalyst mass = 200 mg; total flow rate = 200 sccm. For hydrogen kinetics, H_2, ~ 1.0% PAc, balanced with He.

Figure 5. Arrhenius plot of overall TOF over Pd-10. Reactor conditions: P = 1 atm; ~1.0 % PAc, 20% H_2 balanced with He; catalyst mass = 200 mg; total flow rate = 200 sccm

Catalysis Science & Technology Accepted Manuscript

Scheme and Figures

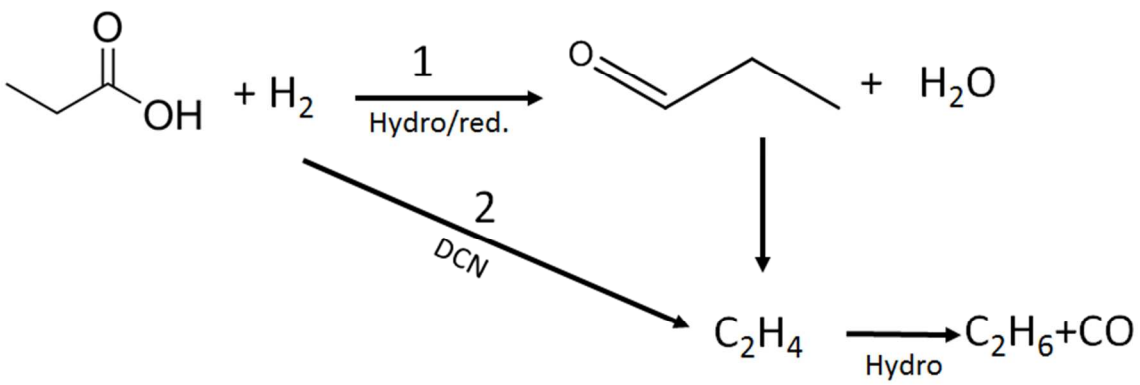

Scheme 1. Reaction pathway for the decarbonylation(DCN)/hydrogenation of PAc over Pd/SiO_2

Catalysis Science & Technology Accepted Manuscript

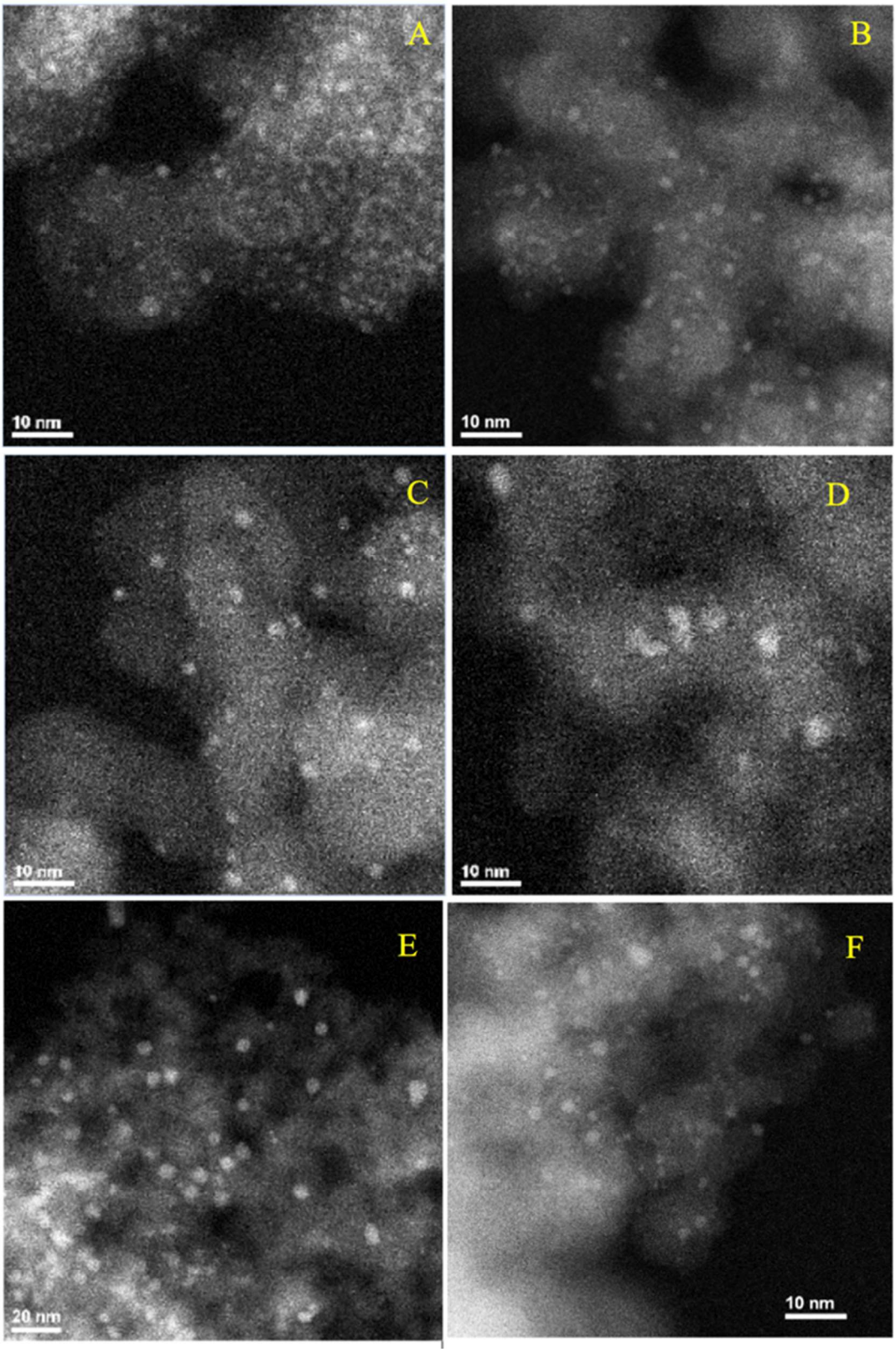

Figure 1. TEM images for Pd-2 before (A) and after (B) reaction, Pd-6 before (C) and after (D) reaction, and Pd-10 before (E) and after (F) reaction

Catalysis Science & Technology Accepted Manuscript

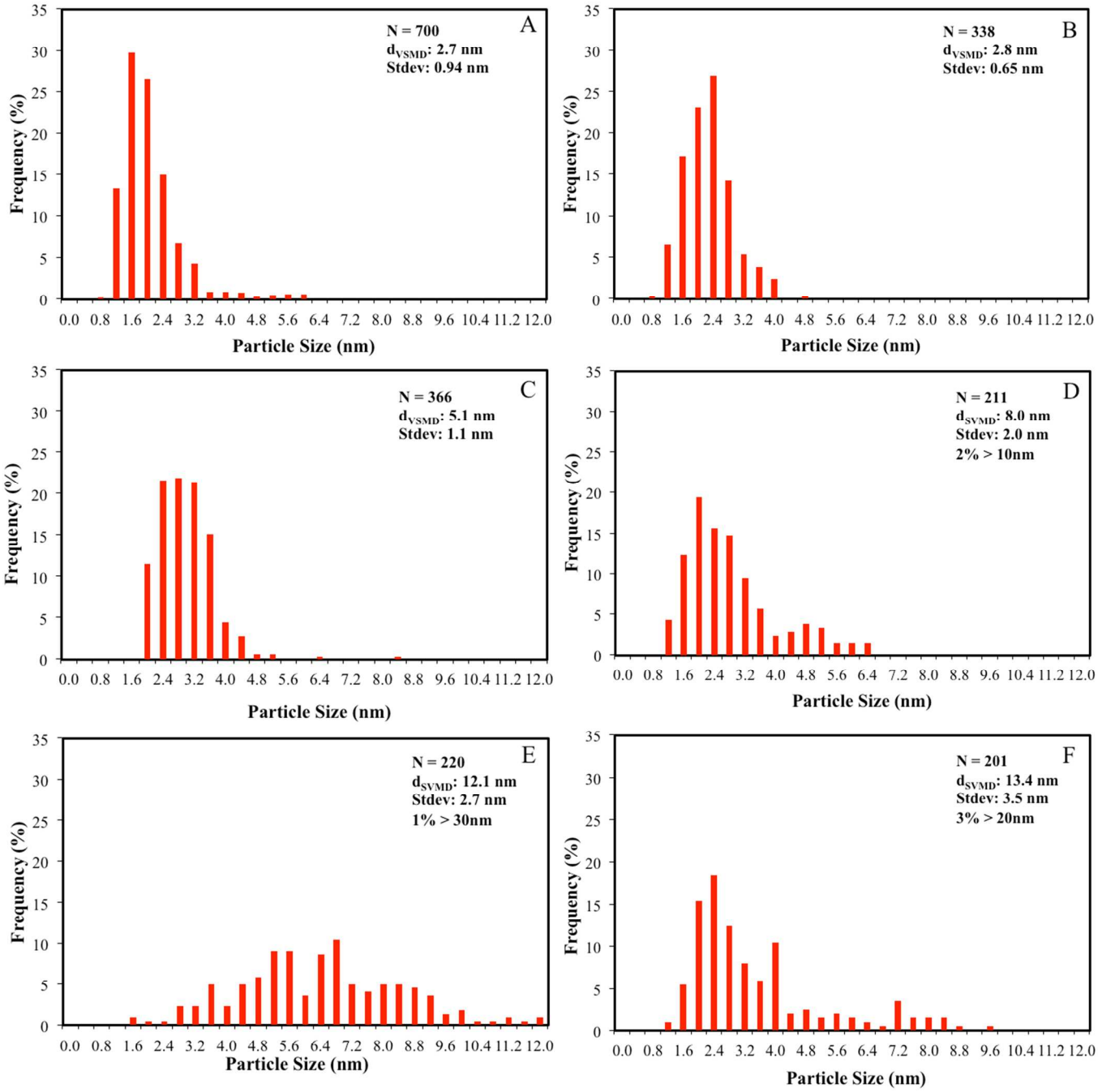

Figure 2. Histograms showing the particle size distributions of Pd-2 before (A) and after (B) reaction, Pd-6 before (C) and after (D) reaction, and Pd-10 before (E) and after (F) reaction. N = Number of particles meaured; D_{VSMD} = volume-surface mean diameter; Stdev = standard deviation.

Catalysis Science & Technology Accepted Manuscript

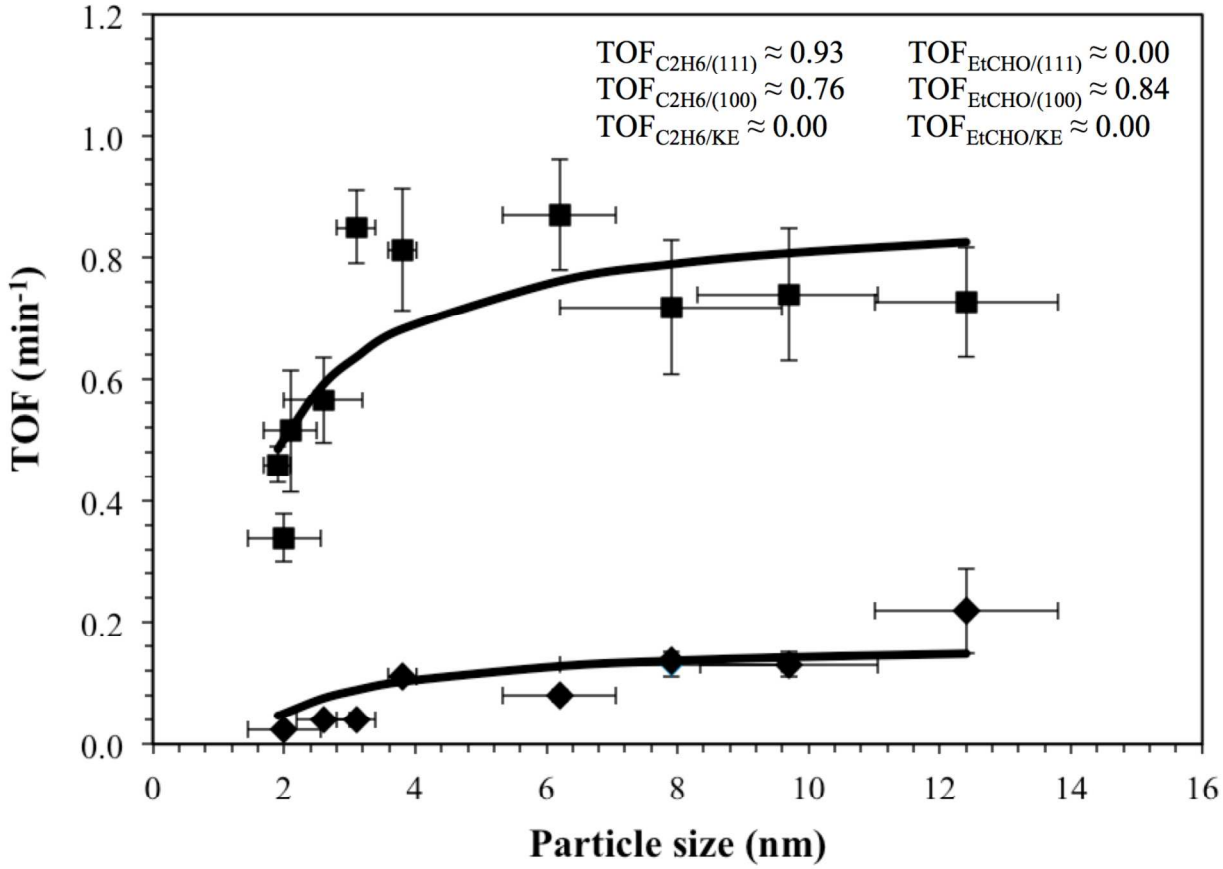

Figure 3. TOF_{C2H6} (squares) and TOF_{EtCHO} (diamonds) as a function of particle size for the series of Pd/SiO_2 catalysts for the HDO of PAc. Reactor conditions: T = 200 ºC; P = 1 atm; ~1.0 % PAc, 20% H_2 balanced with He; catalyst mass = 200 mg; total flow rate = 200 sccm. The solid lines are the least squares fits of the data. See text for details.

Catalysis Science & Technology Accepted Manuscript

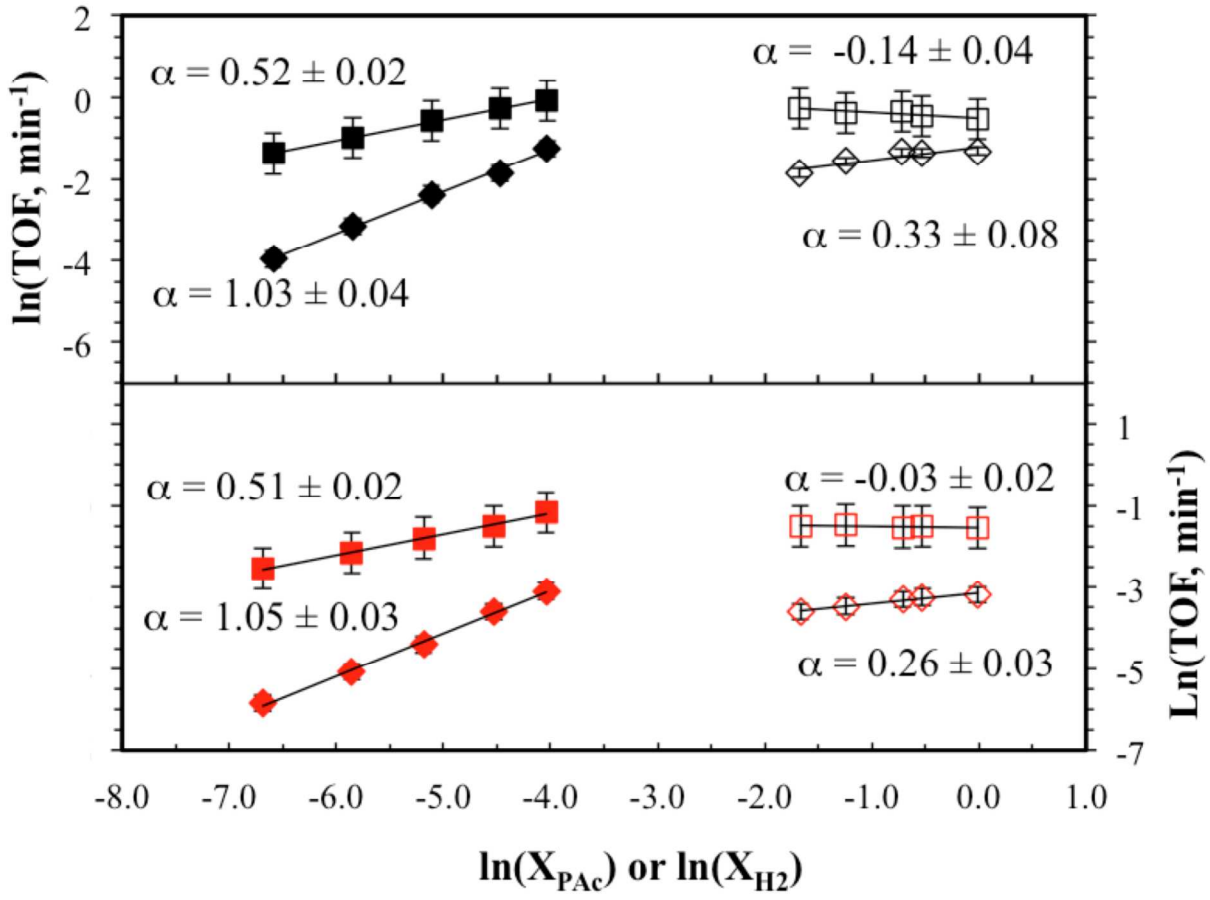

Figure 4. Power rate law dependencies of TOF_{C2H6} (squares) and TOF_{EtCHO} (diamonds) on PAc (filled symbols) and H_2 (open symbols) over Pd-2 (red symbols, bottom plot) and Pd-10 (black symbols, top plot). Reactor conditions: T = 200 ºC; P = 1 atm; PAc, 20% H_2 balanced with He; catalyst mass = 200 mg; total flow rate = 200 sccm. For hydrogen kinetics, H_2, ~ 1.0% PAc, balanced with He.

Catalysis Science & Technology Accepted Manuscript

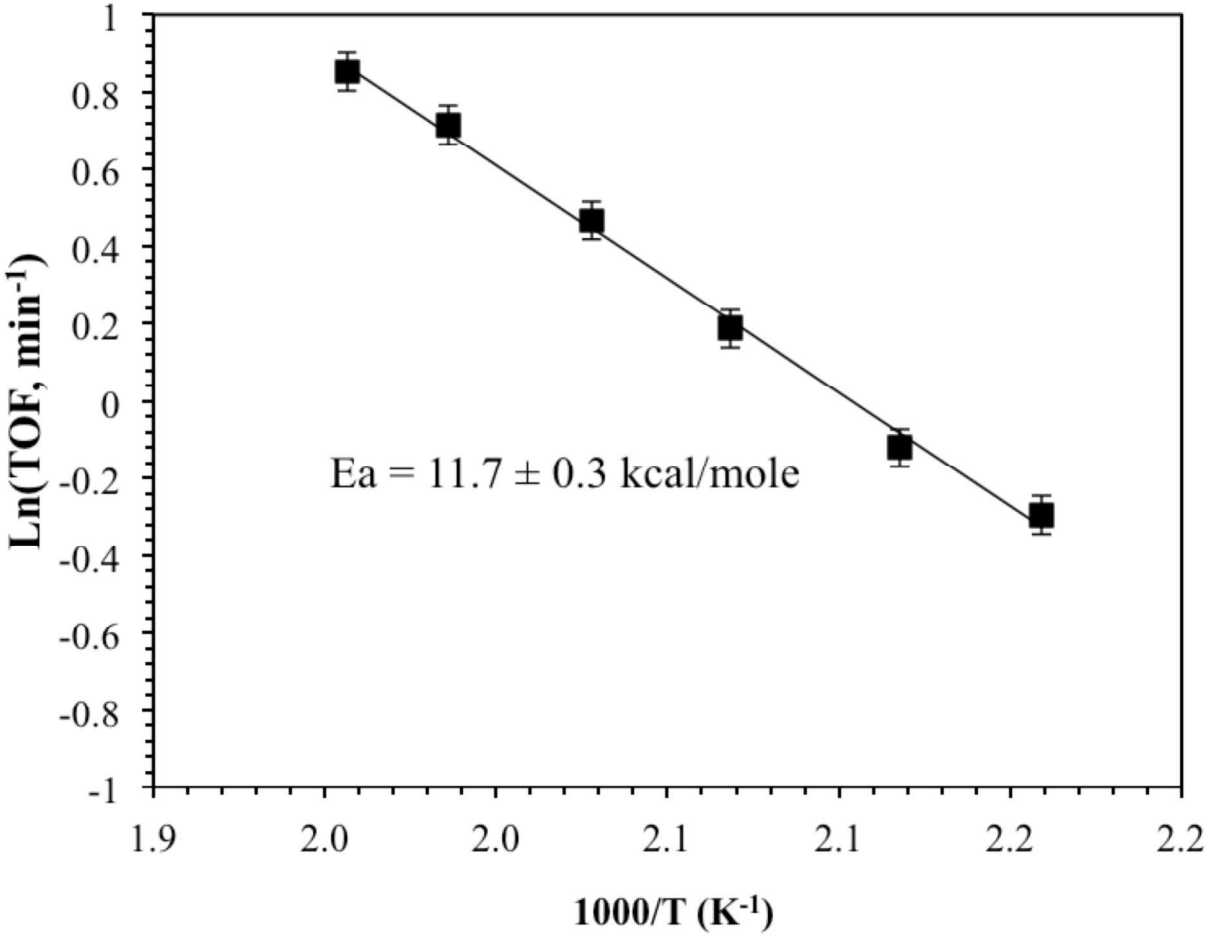

Figure 5. Arrhenius plot of overall TOF over Pd-10. Reactor conditions: P = 1 atm; ~1.0 % PAc, 20% H_2 balanced with He; catalyst mass = 200 mg; total flow rate = 200 sccm

Catalysis Science & Technology Accepted Manuscript